

# VALIDATION OF A NAVIER-STOKES SOLVER FOR AIRFOIL HIGH-LIFT ANALYSIS

Marc Langlois and Farzad Mokhtarian  
Advanced Aerodynamics Dept., Bombardier Aerospace  
Montréal (Québec) Canada

**Keywords:** *high-lift, Navier-Stokes, two-dimensional*

## Abstract

*This paper presents the results of validation exercise of a two-dimensional Navier-Stokes solver conducted for high-lift application by Bombardier Aerospace. The aim of the study was to investigate the capability of the code to accurately predict the complex flows around high-lift configurations and the requirements in terms of mesh density and turbulence modelling for successful computations. The experimental data for this validation comes from a dedicated two-dimensional high-lift test conducted in January 2001 in the Canadian Institute for Aerospace Research (IAR) high-Reynolds number 15 in. × 60 in. test facility. Three test cases have been selected from the experimental data: a clean airfoil, a slat-deployed configuration and a flap-deployed configuration. The parameters that were investigated included the extent of the computational domain, the wall spacing, local mesh refinement and modelling. Guidelines for the successful computation of airfoil high-lift flows are deduced from this study.*

## 1. Introduction

Over the last decade, Bombardier Aerospace has designed and put into production a number of regional and business aircraft that are world leaders in their class. As the complexity of the high-lift systems increased, increasingly sophisticated CFD analyses were used to design efficient multi-element airfoils and wings. For two-dimensional and three-dimensional analyses, current methods cover the whole range

from panel method to Navier-Stokes solvers. While viscous panel methods and Euler/boundary-layer codes are still the main tool for wing design, Navier-Stokes codes are routinely used today for airfoil design. However, the requirements in terms of discretization as well as transition specification and turbulence modelling for accurate predictions of maximum lift ( $C_{L\max}$ ) and lift-to-drag ratio ( $L/D$ ) still remain to be clearly established. The challenge for CFD lies with configurations with closely coupled elements inducing complex phenomena such as wake merging and impingement, channel-like flow and large recirculating/stagnant flow regions [1, 2]. The aim of this paper is to present a validation exercise of a 2-D Navier-Stokes solver for such configurations using data from a recent two-dimensional high-lift wind tunnel test.

## 2. Test facility

The testing was conducted in the Institute for Aerospace Research (IAR) high-Reynolds-number 5'x5' trisonic wind tunnel located in Ottawa. This blow-down tunnel has a 15'x60" two-dimensional test section. It can operate at unit Reynolds numbers up to  $40 \times 10^6$  per foot. The instrumentation available included a 3-component strain gauge balance for the measurement of forces and moments and a traversing wake rake for the determination of the drag from the total pressure deficit in the wake. Lift was mostly obtained through the integration of the pressure distribution measured along the model centreline. Additional information regarding the wind tunnel

capabilities can be found in References 3 and 4.

### 3. Model Description

The model was designed to fit into the 2D insert of the wind tunnel at IAR. It had a clean airfoil chord of 10 inches and a span of 15 inches, based on a Bombardier Aerospace experimental supercritical airfoil (see Figure 1). The airfoil maximum thickness-to-chord ratio ( $t/c$ ) was 0.106. In addition to clean leading and trailing edges, the model was designed with a 16%-chord leading edge slat that could be deflected to between  $15^\circ$  and  $30^\circ$  and a 23%-chord double-slotted hinged flap with a fixed 6%-chord vane, deflectable from  $0^\circ$  to  $40^\circ$ . Five butte door positions were available from  $0^\circ$  to  $31^\circ$ . The model was instrumented with pressure taps running chordwise along the centreline (53 on the main element, 12 on the slat, 4 on the vane and 22 on the flap) as well as a spanwise row of taps near the flap trailing edge to check for two-dimensionality. A discussion of selected experimental findings can be found in Reference 5.

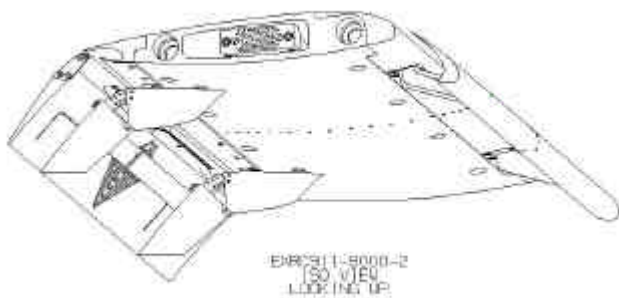


**Figure 1: 2-D high-lift model (slat and flap deployed)**

### 4. Description of the solver

NSU2D [6,7] is an unstructured-grid compressible 2-D solver developed by D.J. Mavriplis. It solves the Reynolds-averaged Navier-Stokes equations using a Galerkin finite-

element approach. Flow and turbulence variables are stored at the vertices of the mesh. The convective fluxes are computed at the vertices and assumed to vary linearly of the triangular elements, while the velocity gradients in the viscous stresses are computed at the centers of the triangles with the flow variables assumed to vary linearly over the triangles. The discretized mean flow equations are integrated in time using an explicit five-stage Runge-Kutta scheme devised to ensure rapid damping of high-frequency errors. Convergence acceleration techniques include local time stepping and implicit residual smoothing as well as the use of an algebraic multigrid algorithm.

Four different turbulence models are available: the Baldwin-Barth and Spalart-Allmaras one-equation models and the  $k-\varepsilon$  (with and without wall functions) and Menter's baseline  $k-\omega$  two-equation models. A point-implicit iteration scheme is used to solve the turbulence equations.

Grid generation is performed with the accompanying software with coarse grid levels generated automatically. In the mesh generation process, highly-stretched elements are first generated in the boundary layer and wake regions using an advancing-layer method. The remaining regions of the field are then filled with isotropic triangles using an advancing-front Delaunay triangulation scheme. Wake lines are constructed using a panel method or can be defined externally by the user. The surface mesh density is controlled by specifying the desired spacing at selected control points. In addition, the mesh is automatically refined in regions of high surface curvature and where curves come in close proximity to one another. Point sources can also be used in the interior of the computational domain to control the mesh density locally.

### 5. Clean airfoil configuration

The influence of some basic mesh and solver parameters was first investigated on a clean

airfoil configuration at a relatively high incidence of 14 degrees. Clearly, we need to establish the capability of the solver to predict stall and maximum lift. However, stall is triggered by flow separation, which, even on a nominally two-dimensional test configuration is a three-dimensional phenomenon. Inspection of the spanwise pressure distributions near the airfoil trailing edge shows that the 2-D nature of the flow is often lost before maximum lift is attained, and the margin increases with slat and flap deflection. This information was used to select test cases for which the comparison with 2-D predictions is still valid. Figure 2 shows an example of spanwise pressure distributions and the loss of two-dimensionality with incidence.

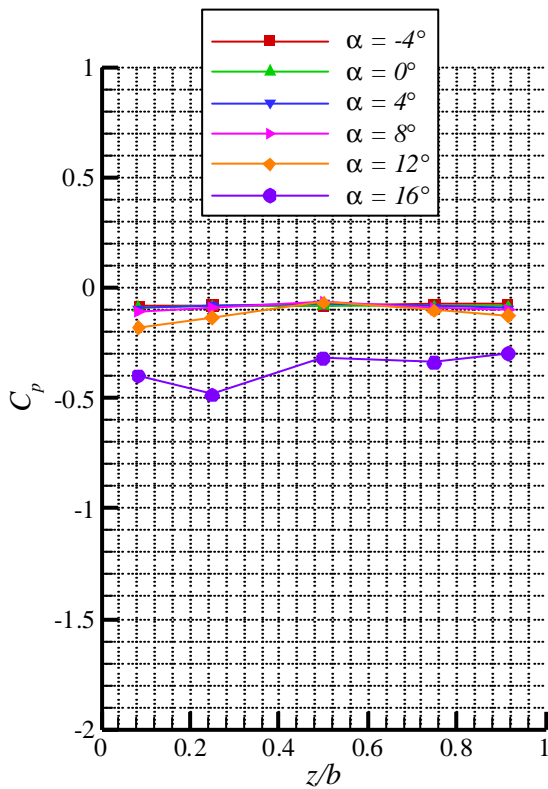


**Figure 2: Spanwise pressure distribution near airfoil trailing edge**

The dependence of the solution on computational domain size is illustrated in Figure 3, which shows the variation of the lift coefficient with the distance of the far-field boundary from the airfoil, expressed in airfoil chords. Even though NSU2D incorporates a circulation correction on the far field, it is clear

that a 10-chord distance for the far-field boundary is not enough to guarantee a numerically accurate solution. The following computations were thus performed on meshes with a far field boundary 30 chords away from the airfoil surface.

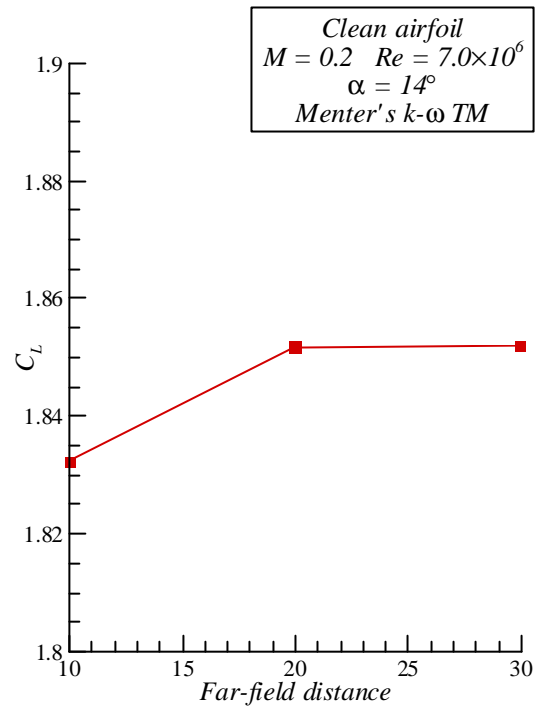


**Figure 3: Lift variation with far-field distance, clean airfoil**

When computing turbulent flows, the normal spacing of the mesh away from the surface has a significant influence on the solution. A wall spacing of  $10^{-6}$  times the chord is the commonly used in the literature. Figure 4 shows the pressure distributions obtained with this spacing and spacings 10 times smaller and larger. Whereas decreasing the spacing does not change the solution, thereby showing that the  $10^{-6}$  spacing is indeed adequate, increasing it results in a lower suction peak and a small trailing edge separation bubble which is otherwise not present. The normal spacing has an even stronger influence on the skin friction distribution, as shown in Figure 5, and hence on the drag prediction. All other computations presented in this paper used a normal spacing of  $10^{-6}$  times the reference chord of the airfoil. It was verified in all cases that this spacing

resulted in a value of  $y^+$  at the wall smaller than 1 over most of the airfoil.

The results presented so far were obtained using Menter’s baseline  $k-\omega$  turbulence model. Figure 6 shows the influence of the turbulence model on the pressure distribution for this test case. The pressure peak on the airfoil seems to be slightly better predicted with the one-equation Spalart-Allmaras turbulence model, but this difference is very small. On the other hand, the  $k-\omega$  model matches the experimental trailing edge pressure distribution better than the one-equation model, which shows a separation bubble. It should be noted that this bubble does not disappear when the Spalart-Allmaras model is used on the mesh with the finer wall spacing.

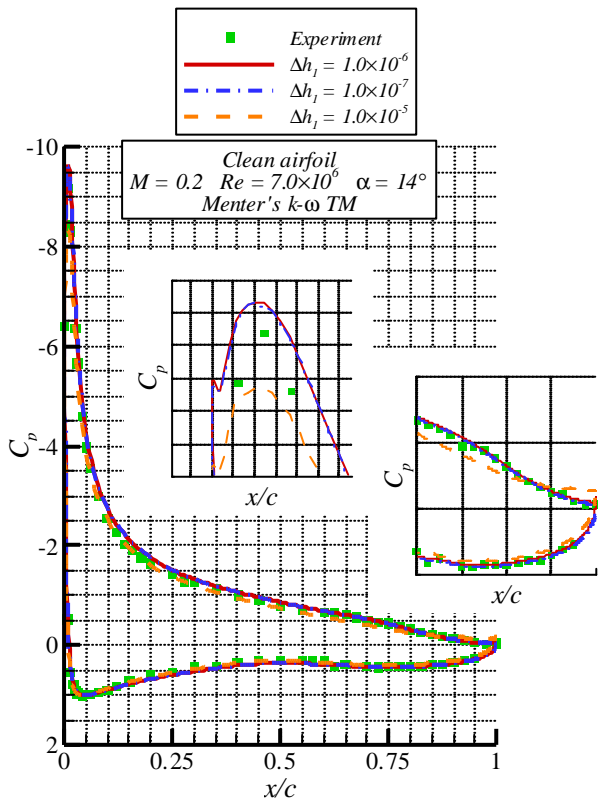


**Figure 4: Influence of mesh normal spacing on pressure distribution, clean airfoil**

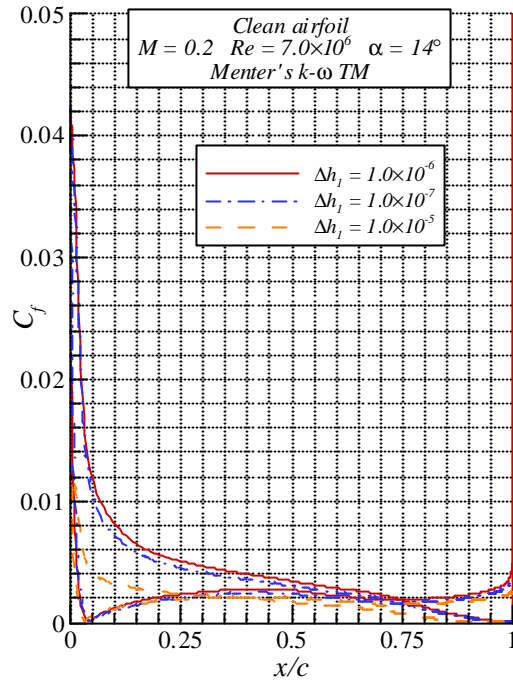


**Figure 5: Influence of mesh normal spacing on skin friction distribution, clean airfoil**

## 6. Slat-deployed configuration

The presence of a slat gives rise to a large region of recirculating flow. At small slat deflections, there is also an important channel effect and the possibility of wake impingement on the main airfoil. A configuration with a slat deployed at  $20^\circ$  and a stowed flap was chosen for this test case, in order to isolate the effect of the slat from that of the flap. Figure 7 shows close-up views of 3 meshes used in this study. For the initial mesh, spacings were specified only at the trailing edge of each airfoil; the only local refinement was that based on surface curvature. On the second mesh, additional control points were imposed in order to refine the mesh on the lower forward portion of the main. Finally, the third mesh combines the surface refinement with refinement in the mesh volume with specification of interior point sources between the slat and the main element.

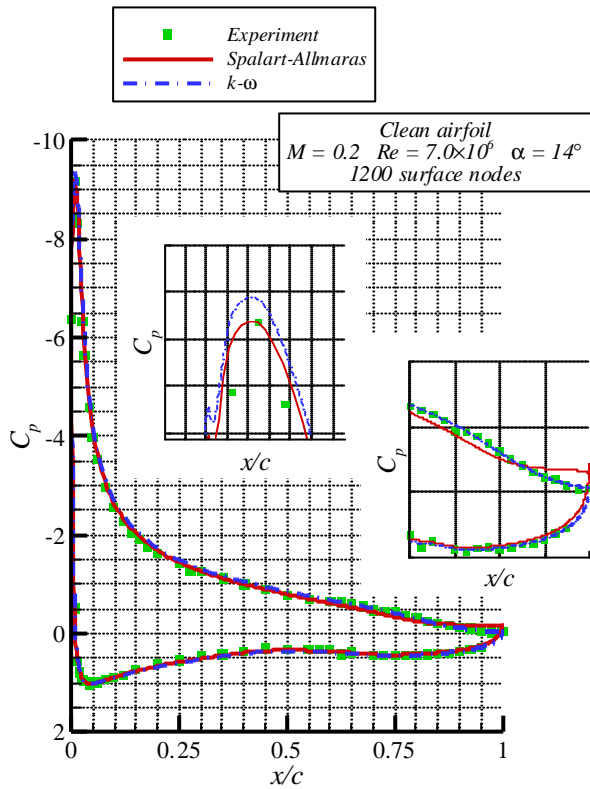


**Figure 6: Influence of turbulence model on pressure distribution, clean airfoil**

The pressure distributions computed on these meshes with the  $k-\omega$  turbulence model are compared to the experimental data for an incidence of  $4.90^\circ$  in Figure 8. All computations show very good agreement with the wind tunnel measurements on the main airfoil upper surface and over most of the lower surface. Up to 25% chord on the lower surface, the predictions on the initial mesh do not match the experimental data as well. This corresponds to the portion of the airfoil that is affected by the recirculation behind the slat. Refining the surface mesh in this area brings a considerable improvement in the agreement. The volume refinement brings an additional improvement, but one which may not be large enough to justify the additional grid generation and computational work. On the slat, the pressure distribution in the cove is also improved when the surface mesh is refined, with a nearly-constant freestream pressure, and the volume refinement does not provide any improvement.

The influence of the slat wake modelling in the grid was also investigated. This was done to see whether the improvement obtained by the mesh volume refinement could be replicated by refining the mesh along the wake emanating from the slat lower lip, as shown in Figure 9. Currently, only a single wake line can be specified per element, and the previous results were obtained with a wake extending from the slat trailing edge over most of the main airfoil upper surface. To isolate the effect of removing this wake, computations were also performed on a mesh without any wake line from the slat.

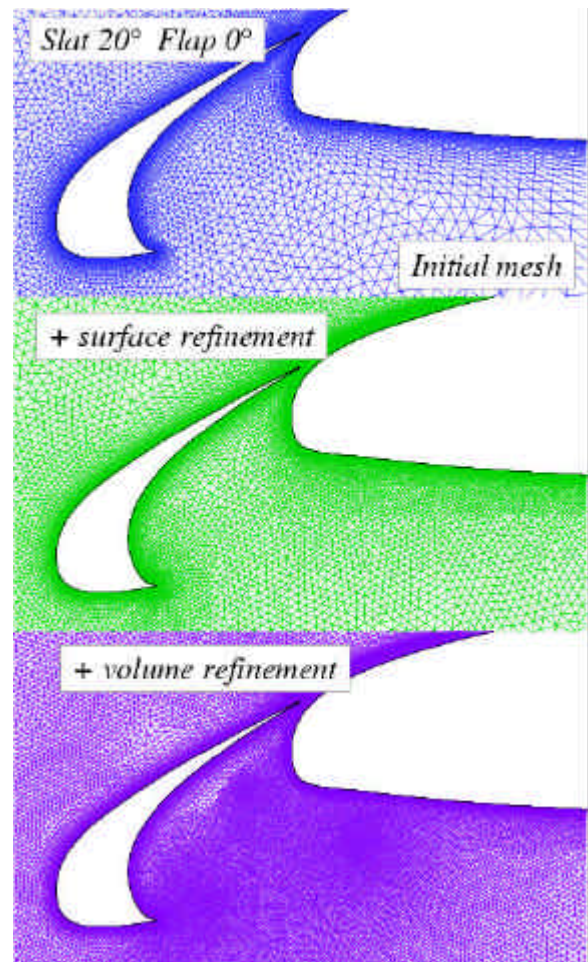


**Figure 7: Mesh refinement study, slat-deployed configuration**

The results of these computations are shown in Figure 10. Removing the trailing edge wake is seen to have no influence on the solution: the mesh in the region where the wake was is still refined in the normal direction, due to the presence of the stretched cells from the

main airfoil upper surface which is allowed to grow further without the wake constraint. The situation might be different if the slat and its wake were further from the main airfoil. The modelling of a wake from the slat lower lip, on the other hand, has an effect opposite to that expected as it deteriorates the agreement of the numerical results with the experimental pressure distribution. This may, however, be due to the poorer convergence of the computations in this case.

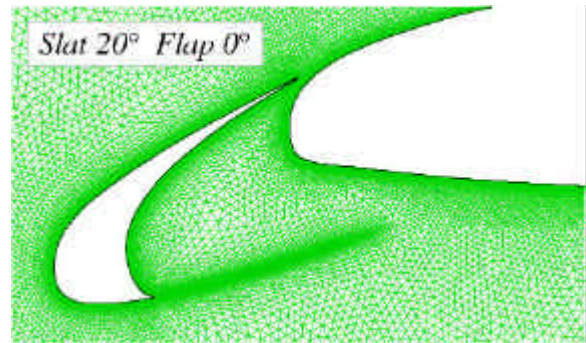


Figure 9: Mesh with wake from slat lower lip

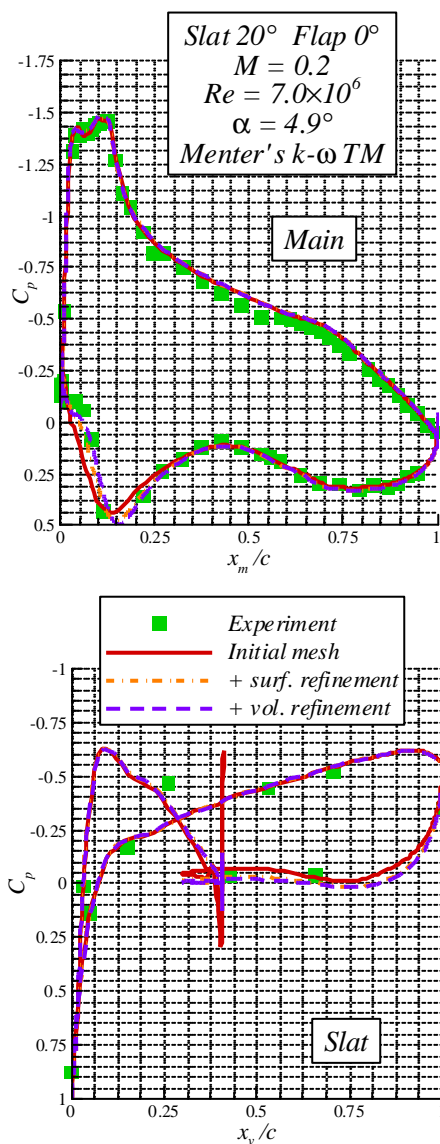


Figure 8: Influence of mesh refinement on pressure distribution, slat-deployed configuration

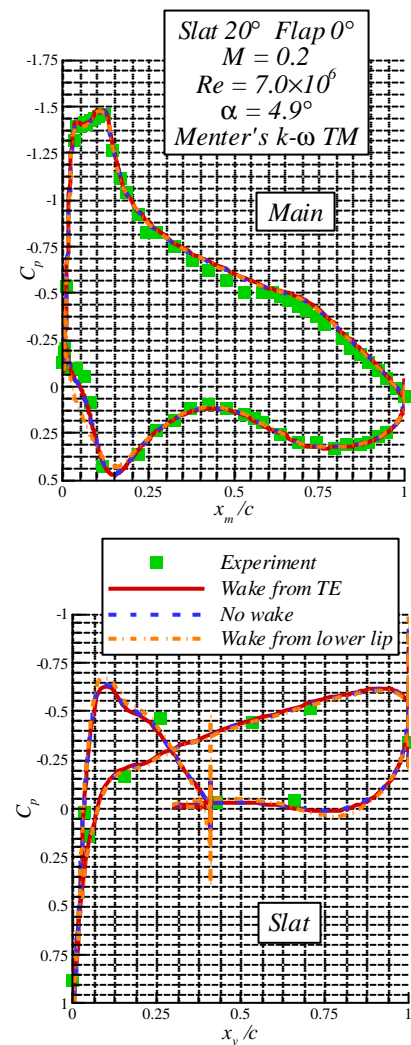
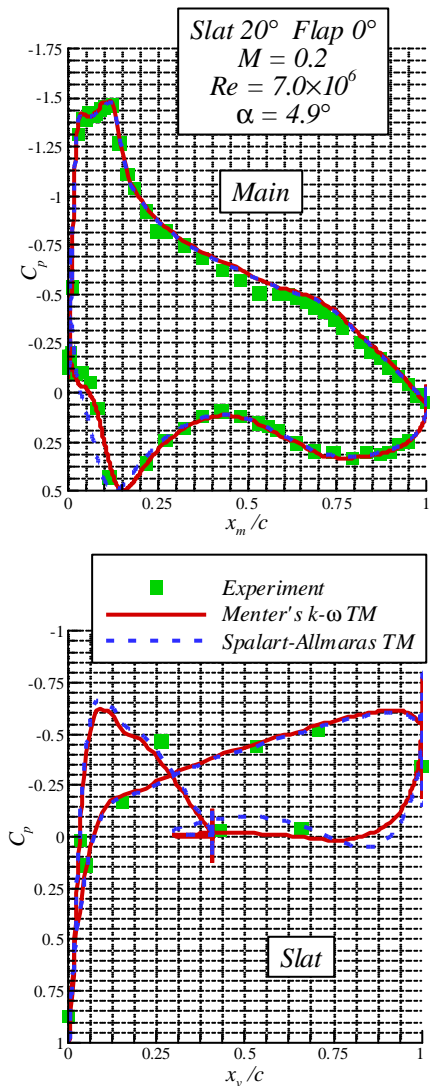


Figure 10: Influence of slat wake on pressure distribution

The comparison of the results obtained with the  $k-\omega$  and Spalart-Allmaras turbulence models is presented in Figure 11. These computations were performed on the mesh with surface refinement only. As should be

expected, the two-equation turbulence model is superior to the one-equation one in predicting the pressure in the recirculation region behind the vane. In particular, the Spalart-Allmaras model does not predict a constant  $C_p$  (zero) in the slat cove, as does the  $k-\omega$  model.



**Figure 11: Influence of turbulence model on pressure distribution, slat-deployed configuration**

### 7. Flap-deployed configuration

The proper modelling of the flow around the flap strongly influences the overall pressure distribution over the complete configuration. The configuration selected for this test case has

a clean leading edge and a flap deflected to  $26.67^\circ$ . In this configuration, the vane is less than halfway out of the main airfoil cove; there is a narrow channel between the vane upper surface and the cove and the vane leading edge is close to the bute door trailing edge which is deflected up by  $31^\circ$ , as shown in Figure 12. This makes it a challenging test for the solver.

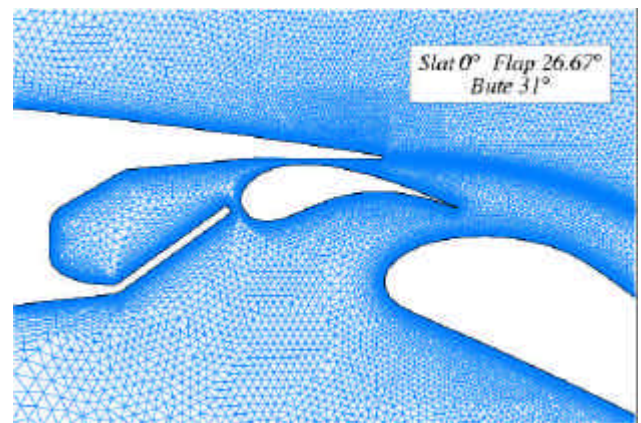


**Figure 12: Flap-deployed configuration**

Figure 13 shows the flap pressure distribution computed on this configuration using the two-equation turbulence model at an incidence of  $7.04^\circ$ . There is considerable disagreement between this solution and the experimental data, especially in the shape of the pressure distribution on the flap and on the rear portion of the main element. Attempts at improving the predictions by refining the mesh or changing the turbulence modelling failed to produce any better agreement.

The flow pattern in the vicinity of the vane is depicted in Figure 14, which shows significant flow through the bute door-vane gap, creating a strong circulation around the vane. A similar flow pattern around the vane was observed in NSU2D predictions on the CRJ-700 for a configuration very much like this one. The predicted flap pressure distribution in that case was also similar to the one seen here and matched flight test data well. On the other hand, results from panel and Euler/boundary layer codes where the gap between the vane and

the bute door is not modelled showed flap pressure distributions more like the experimental one presented here. It was then hypothesized that the circulation around the vane, predicted by the Navier-Stokes code and not by the others, was responsible for the better agreement with the flight test data. This led to the assumption that in the present case, the bute door-vane gap got blocked in the wind tunnel, thus preventing the establishment of circulation around the vane and resulting in the observed flap pressure distribution.

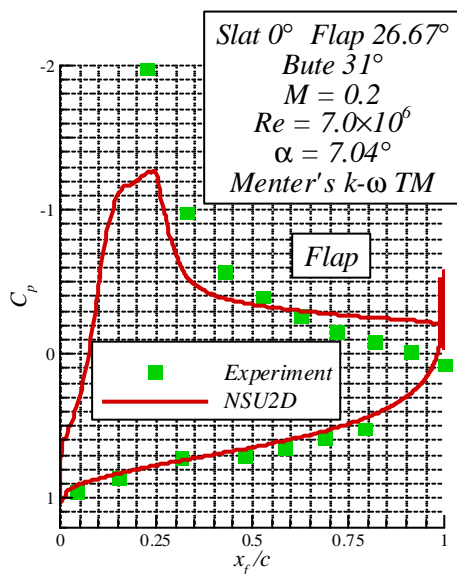


Figure 13: Flap pressure distribution, nominal geometry

To test this hypothesis, a mesh was generated in which the vane and bute door were joined together, as shown in Figure 14. The results of the computations are shown in Figure 16, where the solution on the modified geometry corresponds to the curve labelled “vane closed”. These show a much-improved agreement with the wind tunnel data, on both the flap and main element. The suction peak on the flap could probably be further improved by local mesh refinement. This illustrates the fact that relatively small deviations from the nominal geometry can have significant effects on the flow, especially when gaps and channel-like flows are involved.

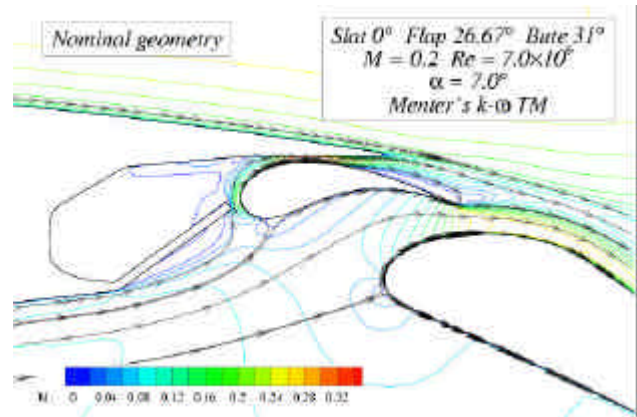


Figure 14: Flow pattern near vane, flap-deployed configuration, nominal geometry

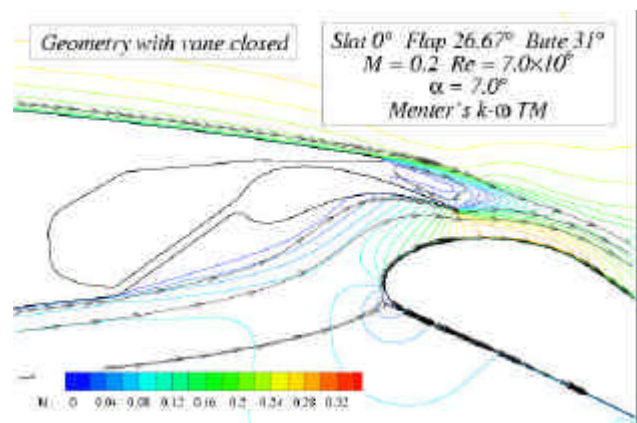
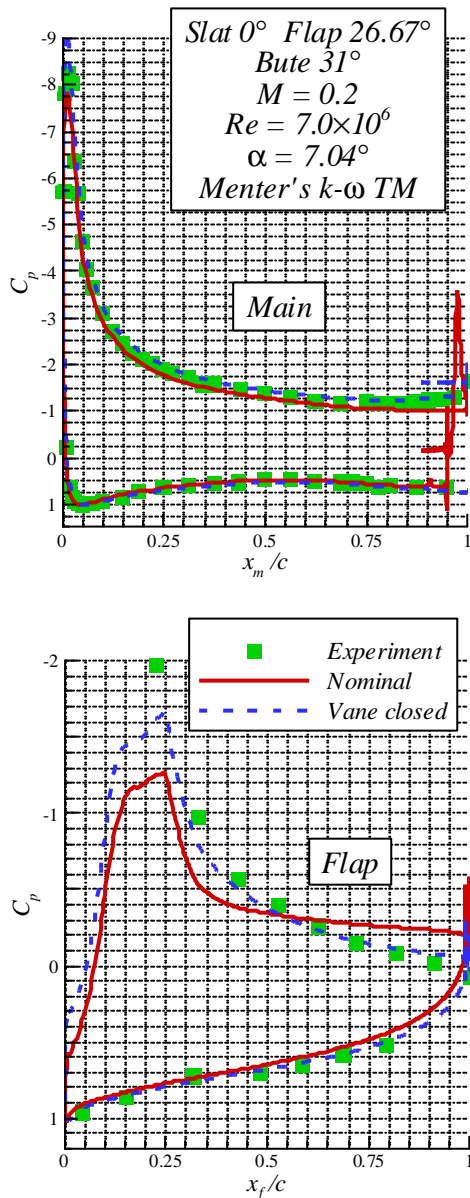


Figure 15: Flow pattern near vane, flap-deployed configuration, geometry with vane closed

## 8. Conclusions

Selected comparisons of two-dimensional Navier-Stokes predictions with the data from a 2-D high-lift wind tunnel test have been presented. The aim of this study was to investigate the ability of the NSU2D Navier-Stokes solver to properly predict the complex flow phenomena around multi-element airfoils and to establish some guidelines for its successful application. Three test cases were used in this study, consisting of a clean airfoil, a slat-deployed configuration and a flap-deployed configuration.



**Figure 16: Influence of vane modelling on pressure distribution, flap-deployed configuration**

Regarding mesh density, the following recommendations can be made. For the same surface density, the computational domain should extend at least 20 to 30 chords from the airfoil surface to insure a mesh-converged solution. For Reynolds numbers of the same order as that considered here, a mesh spacing in the normal direction of  $10^{-6}$  times the chord is sufficient to obtain an adequate value of  $y^+$  of the order of 1. Using a larger wall spacing

results in the erroneous prediction of a trailing separation bubble on the clean airfoil and much reduced skin friction coefficients near the leading edge. Mesh refinement based on curvature alone may not be sufficient to capture all flow features. In particular, user-specified local mesh refinement is necessary on the surfaces in the recirculation regions. Volume refinement through interior point sources does not seem however to provide a significant additional improvement in this case. The modelling of a wake from the lower lip of the slat does not appear to improve the quality of the predictions. All of these point to the fact that mesh adaptation could be a very useful tool for accurate high-lift flow predictions. The selection of a quantity on which to adapt the mesh in separated flow regions may however pose a problem

Concerning turbulence modelling, the results presented point to the superiority of the two-equation  $k-\omega$  model over the one-equation Spalart-Allmaras model for high-lift applications. The latter tends to predict trailing edge separation ahead of the former and of the experimental measurements. With the slat deployed, the location of the main airfoil attachment point and the pressure on its forward lower surface and in the slat cove are also better predicted with the two-equation model.

This study does not claim to be exhaustive. It is part of an on-going effort within Bombardier Aerospace to gain confidence in Navier-Stokes methods and apply them to more and more applications of increasing complexity.

**Acknowledgments**

The experimental part of this project was conducted jointly with the Institute of Aerospace Research (NRC), which funded half of the wind tunnel test. The collaboration of all IAR staff involved in the test is gratefully acknowledged.

## References

- [1] Valarezo, W.O. and Mavriplis, D.J. Navier-Stokes applications to high-lift airfoil analysis. *Journal of Aircraft*, Vol. 32, No. 3, pp. 618-624, 1995.
- [2] Lynch, F.T., Potter, R.C. and Spaid, F.W. Requirements for effective high lift CFD. *Proceedings of the 20<sup>th</sup> Congress of the International Council of the Aeronautical Sciences*, Sorrento, Italy, Vol. 2, ICAS Paper 96-2.7.1, pp. 1479-1492, 1996.
- [3] Galway, R.D. The IAR high-Reynolds number two-dimensional test facility - A description of equipment and procedures common to most 2-D airfoil tests. NRC Aeronautical Note IAR-AN-66, NRC No. 32123, 1990.
- [4] Ohman, L.H. et al. The NAE high Reynolds number 15 in.×60 in. two-dimensional test facility. Part 1: General information. NRC Technical Report LTR-HA-4, 1970.
- [5] Langlois, M., Kho, C.K., Mokhtarian, F. and Kafyeke, F. Investigation of a multi-element airfoil high-lift characteristics at high Reynolds numbers. *Proceedings of the 8<sup>th</sup> CASI Aerodynamics Symposium*, Toronto, Canada, pp. 387-396, 2001.
- [6] Mavriplis, D.J. and Jameson, A. Multigrid solution of the Navier-Stokes equations on triangular meshes. *AIAA Journal*, Vol. 28, No. 8, pp. 1415-1425, 1990.
- [7] Mavriplis, D.J. and Martinelli, L. Multigrid solution of compressible turbulent flow on unstructured meshes using a two-equation model. *Int. Journal for Numerical Methods in Fluids*, Vol. 18, pp. 887-914, 1994.